Nat. Hazards Earth Syst. Sci. Discuss., https://doi.org/10.5194/nhess-2017-98
Manuscript under review for journal Nat. Hazards Earth Syst. Sci.
Discussion started: 13 June 2017

Natural Hazards and Earth System Sciences
Discussions

Three-dimensional hydrodynamic lake simulations of avalanche-generated impulse wave dynamics for potential GLOF scenarios at Lake Palcacocha, Peru

Rachel E. Chisolm[1], Daene C. McKinney[1]

[1]Department of Civil Architectural and Environmental Engineering, University of Texas at Austin, Austin, TX, USA
Correspondence to: Rachel E. Chisolm (rachel.chisolm@gmail.com)

Keywords: Glacier lake outburst flood, Glacial lake, Lake hydrodynamics, Lake Palcacocha, Peru, Avalanche-generated waves

Abstract. This paper studies the lake dynamics for avalanche-triggered glacial lake outburst floods (GLOFs) in the Cordillera Blanca mountain range in Ancash, Peru. As new glacial lakes emerge and existing lakes continue to grow, they pose an increasing risk of GLOFs that can be catastrophic to the communities living downstream. In this work, Lake Palcacocha is used as a case study to analyze the upper watershed processes that typically comprise a GLOF event, specifically the lake dynamics when an avalanche produces a large tsunami-like wave that might overtop and erode the lake-damming moraine. Dynamics of avalanche-generated impulse waves were investigated through three-dimensional hydrodynamic lake simulations of potential GLOF scenarios at Lake Palcacocha, Peru. Wave generation from avalanche impact was simulated using two different boundary condition methods. Representation of an avalanche as water flowing into the lake generally resulted in higher peak flows and overtopping volumes than simulating the avalanche impact as mass-momentum inflow at the lake boundary. Three different scenarios of avalanche size were simulated for the current lake conditions, and all resulted in significant overtopping of the lake-damming moraine. The lake model was evaluated for sensitivity to turbulence model and grid resolution, and the uncertainty due to these model parameters is significantly less than that due to avalanche boundary condition characteristics. Although the lake model introduces significant uncertainty, the avalanche portion of the GLOF process chain is the greatest source of uncertainty. To aid in evaluation of hazard mitigation alternatives, two scenarios of lake lowering were investigated. While large avalanches produced significant overtopping waves for all lake-lowering scenarios, simulations suggest that it may be possible to contain waves generated from smaller avalanches if the surface of the lake is lowered.

1 Introduction

Glacier retreat worldwide has resulted in the emergence and growth of glacial lakes that have replaced ice in the tongue area of many glaciers, and a large number of these lakes pose a risk of glacial lake outburst floods (GLOFs). GLOFs are common in many parts of the world, and they can be catastrophic to downstream communities and infrastructure. Emmer et al. (2016a) have compiled a worldwide database of GLOF events, including approximately

Nat. Hazards Earth Syst. Sci. Discuss., https://doi.org/10.5194/nhess-2017-98
Manuscript under review for journal Nat. Hazards Earth Syst. Sci.
Discussion started: 13 June 2017

Natural Hazards and Earth System Sciences
Discussions

20 events in the Peruvian Andes. Wang et al. (2015b) found that glacial lakes in the central Himalaya have expanded significantly (122.1%) from 1976 to 2010, and Schwanghart et al. (2016) analyzed hydropower installations in the Himalaya and found that about 257 hydropower plants are exposed to GLOF risk. Allen et al. (2016) performed a first-order assessment of GLOF risk across the Himalayan state of Himachal Pradesh (HP), Northern India, including locations where future lakes might form. They identified areas with potentially high GLOF risk and determined that GLOF hazard is likely to increase in the future with continued deglaciation. Linsbauer et al. (2016) calculated glacier overdeepenings and predicted the emergence of future lakes in the Himalaya and Karakoram in relation to GLOF risk and found approximately 5000 overdeepening locations that could form significant glacial lakes. Cook et al. (2016) studied glaciers in the Bolivian Andes where a growing number of proglacial lakes have developed as glaciers have receded (about 40% between 1986 and 2014). They identified 25 lakes that pose a potential GLOF threat to downstream communities and infrastructure. The Cordillera Blanca mountain range in Peru has approximately 1900 lakes, and 830 of them have a surface area greater than 5000 m^2 (UGRH, 2014). Of the lakes in the Cordillera Blanca, over 200 are considered new lakes that have formed recently due to glacier retreat (UGRH, 2014). Several GLOFs have occurred in the Cordillera Blanca in recent history, and climate change and accelerated glacial retreat have been increasing the GLOF hazard since the end of the Little Ice Age in the late 1800's (Carey, 2010).

GLOFs can be highly destructive because the peak discharges tend to be several orders of magnitude larger than typical outflows from glacial lakes (Benn and Evans, 2010). Moraine-dammed lakes such as those present in the Cordillera Blanca are particularly susceptible to outburst flooding (Emmer and Cochachin, 2013). According to studies that have established basic methods for evaluating potential glacial lake hazards (e.g., Haeberli et al., 1989; Huggel et al., 2004; Wang et al., 2011; Emmer and Vilímek, 2014; Rounce et al., 2016), the primary characteristics that signify a potentially hazardous glacial lake are the presence of overhanging ice and the likelihood of failure of the distal face of the lake-damming terminal moraine. However, understanding of the physical processes that can trigger a GLOF event is still limited.

Several studies have looked at GLOF events after they have happened and attempted to reconstruct the GLOF characteristics. Worni et al. (2014) and Westoby et al. (2014a) review various methods for modeling a typical GLOF process chain. Some researchers have simulated GLOFs with models of the individual processes in the chain (e.g., Klimes et al., 2014; Schneider et al., 2014; Westoby et al., 2014b; Worni et al., 2014; Wang et al., 2015a; Somos-Valenzuela et al., 2016); however, the lake dynamics remain one of the most problematic processes to simulate. Most previous studies have used two-dimensional shallow water or empirical simulations of wave generation and propagation in the lakes that do not effectively represent the physical processes. One difficulty is the lack of data about real events, so the potential hazard and impacts of a GLOF must be estimated from an analysis of the physical conditions and modeling the basic physical processes without the availability of calibration data (Somos-Valenzuela et al., 2016). It is a significant challenge to predict the impacts of an event that has not yet happened, and predictive simulations inherently carry considerable uncertainty about many event parameters. Nevertheless, this challenge is one that must be undertaken for progress to be made in glacial hazard assessment and analysis of hazard mitigation strategies.

Nat. Hazards Earth Syst. Sci. Discuss., https://doi.org/10.5194/nhess-2017-98
Manuscript under review for journal Nat. Hazards Earth Syst. Sci.
Discussion started: 13 June 2017

Natural Hazards and Earth System Sciences Discussions

The most common GLOF triggers are landslides, avalanches, or ice calving into a lake (Costa and Schuster, 1988; Richardson and Reynolds, 2000; Bajracharya et al., 2007; Awal et al., 2010; Emmer and Cochachin, 2013; Emmer and Vilímek, 2013). These mass movement events can cause large waves that propagate across glacial lakes and may overtop their terminal moraines. Most studies simulating the GLOF process chain have modeled some of the processes separately with the results from one step in the chain being used as inputs to subsequent steps (e.g., Schneider et al., 2014; Westoby et al., 2014b; Worni et al., 2014); however, most have used 2D SWE models to simulate the waves in the lakes.

This paper focuses on the lake dynamics with the objective of gaining a better understanding of the behavior of avalanche-generated waves and the factors that influence overtopping discharges through three-dimensional, non-hydrostatic simulations of the waves. An improved understanding of the dynamics of avalanche-generated waves can help advance predictive modeling of potential GLOF events, thus enabling better evaluation of possible hazard mitigation strategies at potentially dangerous lakes.

1.1 Lake Palcacocha

GLOFs have been a problem in the Cordillera Blanca for many years (Lliboutry, 1977; Reynolds, 2003; Carey, 2010). The most disastrous GLOF event in the Cordillera Blanca in recent history occurred in 1941 when Lake Palcacocha burst, destroying much of the city of Huaraz and killing approximately 1800 people (Carey, 2010; Wegner, 2014). This event received much notice from national and international media and put the issue of GLOFs at the forefront of national attention in Peru. Huaraz is the most populous city in this area with over 100,000 residents (INEI, 2007 census), and it is once again exposed to a potential GLOF from Lake Palcacocha (Somos-Valenzuela et al., 2016). After the 1941 Huaraz flood, the Peruvian government instituted initiatives to reduce the GLOF risk in the Cordillera Blanca through monitoring of glaciers and glacial lakes and implementing lake safety systems (Carey, 2010). These safety systems typically consist of tunnels to control lake levels, reinforced dams or a combination of the two (Portocarrero, 2014). Scientists and engineers in Peru have several decades of experience managing glacial lakes in the Cordillera Blanca and mitigating GLOF risk (Carey, 2010; Portocarrero, 2014), but current lake management practices are based on studies performed decades ago that have not been updated to account for changes that have occurred since then, primarily increased size and water storage in glacial lakes due to changing climate. The lake safety system implemented at Lake Palcacocha in the 1970's was designed for the size of the lake at the time and did not account for potential lake growth. If the present knowledge of climate change existed at that time, perhaps this could have been foreseen; this was not the case, and now the lake is approximately 17 times larger than it was in 1974 (Rivas et al., 2015), rendering the existing lake safety system inadequate for the current lake dimensions (Portocarrero, 2014). The potential threat that Lake Palcacocha currently poses to the residents of Huaraz has been known for many years. Peruvian government institutions have produced several official reports about the situation (INDECI, 2011; ANA, 2013; Valderrama et al., 2013; Espinoza, 2013; INDECI, 2015), and a state of emergency was declared in 2010 (Diario la Republica, 2010; INDECI, 2011). In this paper, Lake Palcacocha is used as a case study to investigate the impact of an avalanche event on the lake dynamics and the ensuing flood hydrograph.

Nat. Hazards Earth Syst. Sci. Discuss., https://doi.org/10.5194/nhess-2017-98
Manuscript under review for journal Nat. Hazards Earth Syst. Sci.
Discussion started: 13 June 2017

Natural Hazards and Earth System Sciences Discussions

Lake Palcacocha (4562 m) is situated in the Quillcay watershed above the city of Huaraz (Fig. 1). Above the lake are the Palcaraju and Pucaranra glaciers. The steep overhanging ice of the glacier termini in contact with the lake makes it extremely prone to avalanche-generated waves. Additionally, the large volume of water contained in the lake provides a serious threat to downstream areas. The lake is surrounded on three sides by glacial moraines, and the lateral moraines are very tall with steep slopes. The southern lateral moraine is prone to landslides into the lake, and a slide from this moraine in 2003 caused minor damage from a wave that overtopped a portion of the terminal moraine (Vilimek et al., 2005). The original lake-damming terminal moraine was mostly destroyed during the 1941 GLOF, and the lake is currently dammed by a smaller moraine that lies about 300 m back from the 1941 breach. A tunnel to maintain a constant lake level of 4562 m (8 m of freeboard) was constructed in 1974 (Reynolds, 2003; Portocarrero, 2014), and two sections of the smaller terminal moraine have been reinforced with concrete to protect them from erosion. Based on a 2009 bathymetric survey, the volume of the lake was approximately 17 million m^3 at that time (UGRH, 2009). The lake has since retreated approximately 200 m more, and siphons are currently being used to temporarily maintain the lake an additional 3-5 m lower; however, during the rainy season, the siphon system is often not able to keep up with the rainfall draining into the lake. A bathymetric survey undertaken in February, 2016, measured a volume of approximately 17.4 x 10^6 m^3 with a water surface elevation of 4562.88 m (UGRH, 2016). Lake Palcacocha has a deep area adjacent to the glacier with a maximum depth of 72 m and a shallow portion with depths mostly under 10 m extending several hundred meters back from the terminal moraine (Fig. 2).

The potential hazard due to an outburst flood from Lake Palcacocha has been studied by several researchers. Vilimek et al. (2005) discussed the influence of glacial retreat on hazards at Palcacocha and studied the moraine composition and the potential for landslides from the lateral moraines; they also found seepage at the moraine dam. Emmer and Vilimek (2013) used a generalized methodology for GLOF hazard assessment at Lake Palcacocha and 5 other lakes in the Cordillera Blanca, concluding that Lake Palcacocha had the highest hazard level. Emmer and Vilimek (2014) examined mechanisms of the 1941 and 2003 GLOFs at Lake Palcacocha and compared them to other historic GLOFs in the Cordillera Blanca. Emmer et al. (2016b) evaluated the effectiveness of lake safety systems in the Cordillera Blanca and found that the system at Lake Palcacocha resulted in a minimal decrease in GLOF susceptibility. Rivas et al. (2015) modeled a full moraine collapse using empirical equations and DAMBRK hydraulic simulations, and Somos-Valenzuela et al. (2016) gave the results of simulations of a potential GLOF chain of events and mapped potential hazard levels for the city of Huaraz. The results of this paper are focused on the avalanche boundary conditions, turbulence modeling and grid size; whereas, the Somos-Valenzuela et al. (2016) paper focused on the GLOF process chain modeling and downstream impacts.

1.2 Impulse Waves Generated from Avalanches and Landslides

The dynamics of avalanche or landslide-generated waves are very complex. To complicate matters further, it is very difficult to obtain field measurements of these waves, and most of the data from actual events are estimates based on residual evidence in the field (e.g., run-up on side slopes or moraine erosion). The physical principles governing the mechanics of wave generation and propagation are presented in Dean and Dalrymple (1991). A number of studies

Nat. Hazards Earth Syst. Sci. Discuss., https://doi.org/10.5194/nhess-2017-98
Manuscript under review for journal Nat. Hazards Earth Syst. Sci.
Discussion started: 13 June 2017

have developed empirical models from laboratory simulations and/or field data of avalanche and landslide generated waves (e.g., Kamphuis and Bowering, 1970; Slingerland and Voight, 1979 and 1982; Fritz et al., 2004; Heller and Hager, 2010), but many of the laboratory models use simplified geometries (Heller et al., 2016). Numerical simulations of slide-generated waves have been primarily focused on two-dimensional simulations and simple arrangements (e.g., Rzadkierwicz et al., 1997; Zweifel et al., 2007; Biscarini, 2010; Cremonesi et al., 2011; Ataie-Ashtiani et al., 2011; Ghozlani et al., 2013); but, the two-dimensional shallow water equations (SWE) may not be appropriate for slide-generated waves because of the role that vertical accelerations play in the wave dynamics (Heinrich, 1992; Zweifel et al., 2007). Recent developments in numerical simulations of landslide-generated waves include simulation of multi-phase flows, including a three-dimensional Navier-Stokes Volume of Fluid model (Abadie et al., 2010), a two-phase debris flow model (Kafle et al., 2016), and the application of Smoothed Particle Hydrodynamics (SPH) models (Heller et al., 2016; Wang et al., 2016). However, these studies still focus on simple cases and geometries rather than real-world scenarios. Few researchers have looked at the issue of wave run-up (e.g., Synolakis, 1987 and 1991; Muller, 1995; Liu et al., 2005; Capel, 2015; Romano et al., 2015; Etemad-Shahidi et al., 2016), and most use empirical formulas or simplified approaches for wave run-up calculations, making assumptions about the lake geometry that may not be realistic (e.g., uniform water depth and a regularly sloped dam).

Although models of real events are limited by the lack of validation data, there is clearly a need to move away from simplified cases such as sliding blocks or wedges and progress towards modeling cases that more closely resemble geometries and circumstances in the field. Use of three-dimensional numerical modeling can improve simulations of avalanche-generated waves by avoiding some of the weaknesses of two-dimensional shallow water models. Some of the problems of modeling avalanche-generated impulse waves include: uncertainty in the make-up of the avalanche material (e.g., ratio of snow, ice and rock; density; viscosity) and representation of the mixing and momentum transfer when the avalanche material enters the lake.

2 Methods

A three-dimensional hydrodynamic model, FLOW 3D (Flow Science, 2012), was used to simulate waves generated from avalanches entering the lake and investigate the dynamics of the wave generation, propagation and overtopping. A three-dimensional, non-hydrostatic model was chosen to give as realistic a simulation environment as possible. Although two-dimensional SWE models have been applied to simulations of avalanche-generated impulse waves (e.g., Heinrich, 1992; Zweifel et al. 2007), the size and characteristics of the waves indicate that a three-dimensional model may be more appropriate because of highly variable water depths, wave heights and vertical accelerations. Additional motivation for employing this model is the variable lakebed geometries of many glacial lakes that tend to have sharp discontinuities near their terminal moraines that could significantly affect wave propagation and run-up (e.g., Lake Palcacocha, as seen in Fig. 2). The lakebed topography in the FLOW 3D model was taken from a 2009 bathymetric survey (UGRH, 2009).

The three-dimensional, non-hydrostatic model simulated the formation, propagation, run-up and moraine overtopping of an avalanche-generated impulse wave in a glacial lake. The sensitivity to the turbulence model and grid size used in the simulations were investigated to determine how much these aspects of the model might

contribute to the overall uncertainty. Wave generation and propagation were studied to gain insights about how this type of wave behaves and what type of model is needed (2D vs 3D and hydrostatic vs. non-hydrostatic) to accurately reproduce avalanche-generated waves of the magnitude typically seen in GLOFs. Two alternative boundary condition methods, representing the avalanche entering the lake, were studied. Three avalanche scenarios that represent a range of likely avalanche sizes were simulated in addition to two lake-lowering scenarios to evaluate hazard mitigation alternatives. The discharge hydrographs resulting from the overtopping waves were the inputs for a debris flow model used to determine the potential impact for the city of Huaraz (Somos-Valenzuela et al., 2016).

2.1 Sensitivity Analysis: Turbulence Model and Grid Size

2.1.1 Sensitivity to Turbulence Model

The FLOW 3D simulations used a three-dimensional, non-hydrostatic numerical scheme and a re-normalization group (RNG) turbulence model with a dynamically computed mixing length; although, several other turbulence models were also tested. The RNG-dynamic mixing length model was chosen as the baseline turbulence model because an appropriate mixing length was unknown due to the highly variable nature of the flow, both spatially and temporally. The sensitivity of the simulations to the turbulence model was tested by running repeat simulations for seven different turbulence models in FLOW 3D, including: (1) RNG-dynamic mixing length (baseline model), (2) RNG-constant mixing length, (3) k-epsilon, (4) Prandtl mixing length, (5) one-equation-constant mixing length, (6) large eddy simulation (LES), and (7) laminar flow. Simulations of models (2) – (7) were compared to the baseline model for the large avalanche, current lake level scenario using the percent difference in maximum wave height, peak overtopping flow rate, and total overtopping volume. Additionally, the root-mean-square deviation (RMSD) between the results of the baseline and the other models was calculated at each time step for the outflow hydrographs and the flow depth at each point within the lake.

Turbulence models (1) – (5) are Reynolds-averaged Navier-Stokes (RANS) eddy viscosity models (Pope, 2000). Model (2) is a variant of model (1) except that it uses a constant mixing length (Yakhot and Orszag, 1986). Model (3) is a two-equation model that uses several standard constants. Models (4) and (5) are the simplest eddy viscosity models used. In FLOW 3D, the constant mixing length defined in models (2) and (5) is a maximum length scale that limits the dissipation of energy, ensuring that dissipation in the models is not underrepresented (Isfahani and Brethour, 2009).

Models (6) and (7) function differently from the RANS eddy viscosity models. Model (6) simulates only the largest scales of turbulence by using a filter to remove the smaller scales, which are accounted for within the model. The filter size is linked to the model grid size, and additional numerical errors can be introduced due to the filter width. The accuracy of model (6) depends on knowledge of the flow conditions so that the filter scale can be defined to allow for most of the large-scale turbulence to be resolved within the model itself rather than in the sub-grid representation of the small-scale turbulence (Pope, 2000). The results from model (6) should be viewed considering these limitations, since the grid size was not determined according to the scale of turbulence that should be resolved in the model. Model (7) ignores turbulence and simulates the flow as entirely laminar. As turbulence tends to dissipate energy, this model will under-represent dissipation.

Nat. Hazards Earth Syst. Sci. Discuss., https://doi.org/10.5194/nhess-2017-98
Manuscript under review for journal Nat. Hazards Earth Syst. Sci.
Discussion started: 13 June 2017

2.1.2 Sensitivity to Grid Size

Model results tend to improve with grid refinement. The grid cell size used for the simulations was selected to allow for sufficient resolution of the topographic and bathymetric features of the glacial lake as well as the dynamic wave features during the wave generation and overtopping phases while also balancing time and computational resources. To assess the impact of grid size on model results, a simulation was run with a coarser grid.

The regular mesh used in the FLOW 3D model consists of 6 m x 5.33 m x 6.5 m grid cells in the x-, y- and z-directions, respectively, spanning distances of 2400 m (x-direction), 800 m (y-direction), and 650 m (z-direction). For the grid size sensitivity analysis, a coarse grid simulation, with double the original cell grid size, was run for the large avalanche source scenario at the current lake level.

For the coarse grid simulations, the water depth at each time step was extrapolated to the finer grid by dividing the coarse grid cells into the equivalent number of cells in the regular mesh, and the water depth from each x-y grid cell of the coarse grid was given to each of the four corresponding fine grid cells. To compare the coarse grid results to the results from the regular model mesh, the root-mean-square error (RMSE) of fluid depth for all grid cells within the lake was calculated at each time step. Additionally, the percent difference in peak overtopping flow rate and total overtopping volume and the RMSE of the outflow hydrograph were calculated for the coarse grid simulation.

2.2 Boundary Conditions: Representing Avalanche Impact

The problem of reproducing an avalanche-generated impulse wave in a hydrodynamic model of a glacial lake is not easy to solve because of the complicated dynamics of mixing and dissipation of energy that occur at the point of impact. The results of avalanche simulations performed in the Rapid Mass Movements (RAMMS) model (Christen et al., 2010; Bartelt et al., 2013), reported in Somos-Valenzuela et al. (2016), were used to generate inputs to the lake model. Two different methods of representing the impact of the avalanche with the lake and the corresponding mass and momentum transfer were tested to determine the sensitivity of the lake model to the boundary conditions. The variability in the results between the two boundary condition methods gives an approximation of the uncertainty associated with the avalanche impact and wave generation.

2.2.1 Avalanche Source

The avalanche source boundary condition method represents the avalanche entering the lake by simulating water flowing from the lower glacier slopes into the lake. The density of the avalanche material that is typical for this type of GLOF, the mixture of snow, rock and ice, is nearly the density of water (Schneider et al., 2014); therefore, water was used in place of the avalanche fluid, and the volume of the water that represents the avalanche was the same as the total avalanche volume. This is the same approach used by Worni et al. (2014) and Fah (2005). The two fluids (water and the avalanche material) have different viscosities, but the model was adjusted to account for the effects of the lower viscosity of water (less dissipation of energy as it flows towards the lake). The depths and velocities of the avalanche entering the lake from the RAMMS model lake were matched in the FLOW 3D model by varying the height at which the initial avalanche fluid volume was released above the lake and the initial depth of the avalanche fluid in the FLOW 3D model. If the mass and momentum of the flow representing the avalanche impacting the lake

are similar in FLOW 3D and RAMMS, then the FLOW 3D simulations should realistically represent the generated wave. Reflected waves may be somewhat different due to the potential settling of the avalanche material that cannot be represented in the FLOW 3D model, but these differences are probably minimal because the magnitude of the reflected wave is much less than the initial wave.

2.2.1 Mass-momentum Source

The second boundary condition method for representing an avalanche impacting the lake was a mass-momentum source. For this method, hydrographs were constructed from the RAMMS avalanche simulations approximating the volumetric flow rate of the avalanche entering the lake by taking the depth and velocity from RAMMS at various points (approximately 10-15 points) along the edge of the lake for each time step. The average avalanche depth, velocity, and flow rate were calculated for each time step. These avalanche hydrographs were slightly altered so that the total volume was equivalent to the avalanche volume, and the resulting adjusted hydrographs were used as the inflow boundary condition of the FLOW 3D model, representing the input of mass and momentum that generates the impulse wave. This was done using the mass-momentum source function in FLOW 3D with the boundary condition defined by the hydrograph and cross-sectional area of the flow entering the lake.

2.3 Wave Characteristics

There are five main phases of an avalanche-generated impulse wave in a glacial lake: (1) wave generation from the avalanche entering the lake, (2) propagation of the wave across the lake, (3) run-up on the damming-moraine, (4) overtopping of the moraine, and (5) reflected wave(s) from the portion of the wave that does not overtop the moraine. The characterization of these phases of an avalanche-generated wave is important because empirical methods have been developed to model wave generation, but wave propagation often cannot be accurately described by simple empirical equations, especially for glacial lakes with varying bathymetry. Wave generation is dependent primarily on the avalanche characteristics and the lake depth at the point of impact; whereas, wave propagation is dependent on initial wave characteristics, lake bathymetry and the surrounding topography.

The primary parameters used to study the wave characteristics were the maximum height of the wave in the lake and the wave height as it overtopped the terminal moraine. The maximum wave height, as a function of distance along the lake, was calculated to assess how the wave changes during the propagation phase and to allow for comparison with the empirical method of Heller and Hager (2010). At this point, the difficulty of model validation and uncertainty quantification must be mentioned. In this work, events are modeled that have not yet occurred, and very little data are available from similar past events that can be used to calibrate or validate model results. The 2010 GLOF that occurred at Lake 513 in the Cordillera Blanca of Peru provides some information to compare results to, but that event occurred at a lake with unique characteristics (solid rock damming-moraine) and there is some discrepancy among the estimates of the avalanche magnitude, wave height and overtopping volume (Carey et al., 2012; Valderrama and Vilca, 2012; Schneider et al., 2014). Therefore, the results of the empirical model (Heller and Hager, 2010) were used to compare with the FLOW 3D hydrodynamic lake modeling.

Nat. Hazards Earth Syst. Sci. Discuss., https://doi.org/10.5194/nhess-2017-98
Manuscript under review for journal Nat. Hazards Earth Syst. Sci.
Discussion started: 13 June 2017

The empirical method of Heller and Hager (2010) for calculating characteristics of impulse waves is based on a database of field measurements and laboratory experiments. If the characteristics of the impulse wave in both the hydrodynamic and empirical models are similar, then there is reason for confidence in the hydrodynamic model results. However, the empirical method is only an approximation based on simplified representations of lake geometry and avalanche characteristics. The method has certain acceptable ranges of variables, such as relative slide density, volume, width, and Froude number, for which the empirical equations hold true. For Lake Palcacocha, all the variables fall within the acceptable ranges except the relative slide width; therefore, the wave characteristics calculated according to this method can be reasonably relied upon to compare with the three-dimensional simulation results, but only to get an idea of the approximate wave dimensions.

2.4 Scenarios

Two sets of scenarios were simulated with the hydrodynamic model: avalanche scenarios and lake-lowering scenarios. To assess the current GLOF hazard, simulations were first run with the current lake level (the baseline level). The baseline level was defined as the lake level controlled by the current outlet works, a tunnel that maintains a freeboard level of 8 m and a water surface elevation of 4562 m. Three avalanche scenarios were used to represent a range of potential avalanche sizes that might impact the lake: small ($0.5x10^6$ m^3), medium ($1x10^6$ m^3) and large ($3x10^6$ m^3). The avalanche characteristics for each scenario are given in Somos-Valenzuela et al. (2016). Second, scenarios with different lake levels were simulated to study how lowering the lake surface might influence the overtopping wave volume and discharge. These scenarios included lowering the lake level 15 m and 30 m from the baseline lake level. These scenarios were selected based on what has been proposed by local government technical specialists in Huaraz as plausible lake risk mitigation strategies.

Each lake level scenario (including the baseline) was simulated for all three avalanche scenarios, forming a total of 9 scenarios; the overtopping volume and outflow hydrograph were computed for each scenario. Lake lowering scenarios were analyzed for reduction in peak overtopping flow rate and total discharge volume. Although the goal of this work is examining lake hydrodynamics, the greater aim is to assess the potential for GLOFs to impact downstream populations. Simulations of downstream inundation and flood intensities can facilitate analysis of lake lowering schemes to reduce GLOF hazard levels. Somos-Valenzuela et al. (2016) evaluated how lake lowering may alter the GLOF impacts in Huaraz for the avalanche source scenarios and found that overtopping volumes of 20,000 m^3 or less would not result in significant flooding in Huaraz. Considering this, a "safe lake level" was defined as a scenario for which the simulated overtopping volume is less than or equal to 20,000 m^3.

3 Results

For each scenario, FLOW 3D was used to model the avalanche-generated impulse wave, from the wave generation to the overtopping phases. For each avalanche event, simulations were run using both boundary condition methods (avalanche and mass-momentum sources), first for the baseline lake level and then for the two lake-lowering scenarios.

Nat. Hazards Earth Syst. Sci. Discuss., https://doi.org/10.5194/nhess-2017-98
Manuscript under review for journal Nat. Hazards Earth Syst. Sci.
Discussion started: 13 June 2017

3.1 Sensitivity Analysis: Turbulence Model and Grid Size

3.1.1 Sensitivity to Turbulence Model

For the large size scenario with the avalanche-source boundary condition and current lake level, the results of using the various turbulence models were compared to the baseline model (1) (RNG-dynamic mixing length). The RMSD (Fig. 3) shows the average difference in fluid depth between the baseline model and each of the other turbulence models. For all models, the highest RMSD values were for times up to 50 s when the water surface is most actively changing as the impulse wave is generated and begins to propagate across the lake. Models (6) (LES) and (7) (laminar) show the most deviation from the baseline model with maximum RMSD values around 2.5 m. It is not surprising that the laminar model shows high deviations from the baseline model because it does not account for turbulence and should be the least dissipative of all the models. This is reflected in the peak flow rate, overtopping volume and maximum wave height (Table 1), which were all higher than the baseline model. The LES model appears to be overly dissipative, giving the lowest values for all parameters used for comparison between the models. It is difficult to say why this is the case, but it could be due to inhomogeneity in the flow or numerical errors due to the filter scale.

Models (2) (RNG-constant mixing length), (3) (k-epsilon) and (4) (Prandtl mixing length) may be more appropriate for this type of simulation. The results from these models more closely align with the baseline model; however, there are still differences in fluid depth between the models. All three models had maximum RMSD values for fluid depth of around 1.8 m; the models approached a steady state (RMSD of approximately 0.5 m) after 200 s when the initial wave overtopped the moraine. The highly variable lake bathymetry and fluid depths make defining an appropriate mixing length difficult and introduce a source of uncertainty in the model; many of the turbulence models require the definition of a mixing length that ensures that the dissipation of energy is not underrepresented in the model. For this reason, model (1) appears to be the optimal choice in this case. Yet, the similarity in the results between the RANS eddy viscosity models (1) – (5) indicates that the uncertainty introduced by the constant mixing length models is relatively insignificant.

The RMSD of the overtopping hydrograph flow rates for each of the turbulence models are given in Table 1 along with additional comparisons of the hydrographs, including the percent difference in peak flow rate and total overtopping volume. The largest differences in flow rate and overtopping volume came from models (6) (LES) and (7) (laminar) with the laminar model producing higher flows and the LES model producing the lowest flow rates. The hydrographs from the other models resembled that of the baseline model. The percent differences in peak flow rate from the eddy viscosity models ranged from around 0.25% for model (4) (Prandtl) to around 3% for model (3) (k-epsilon). The differences in total overtopping volume were a little higher, although all were less than 5%, and the differences in maximum wave height were much less significant for all but model (6) (LES), with most models giving differences less than 2%.

The laminar model (7) is the only model that gave higher flow rates and overtopping volumes than the baseline model, indicating that even if the turbulence model introduces uncertainty into the model results, the results of the baseline model are most likely conservative, giving possibly higher discharges. Considering all the other sources of

uncertainty in the models of the avalanche and wave generation, the turbulence model is one of the less significant sources of uncertainty.

3.1.2 Sensitivity to Grid Size

The RMSE of fluid depth for the coarse grid simulation compared to the regular mesh is a good measure of the error introduced by changing the grid resolution (Fig. 4). The highest errors were in the first 50 s of the simulation time, during the wave generation, propagation and run-up phases. However, there was a baseline level of error that comes simply from extrapolating the initial conditions to a coarser grid because the bathymetry and initial fluid depths are better represented in the fine grid model. The RMSE at $t = 0$ reflects this error. After 50 s, the RMSE began to level off at a relatively consistent level of approximately 1.5 m. This was about three times higher than the RMSD from the eddy viscosity turbulence models at the same point in time, indicating that grid size could introduce much more error than the turbulence model.

The RMSE of overtopping discharge for the coarse grid simulation was approximately 3300 m^3/s. This amount of error is not insignificant; it is approximately three times the RMSD for the eddy viscosity turbulence models but less than the RMSD for the laminar flow model. The peak discharge from the coarse grid simulation was over 5% higher than the peak discharge from the regular grid size model (a difference of 4,200 m^3/s). The total overtopping volume was slightly higher for the coarse grid simulation (a difference of 30,000 m^3), but the difference was less than 1%, so the coarse grid model seems to estimate the total overtopping volume well even if it does not get the wave dynamics and outflow hydrograph completely correct. Although the error resulting from using a coarser mesh was greater than the uncertainty from most of the turbulence models, the uncertainty due to the grid size is still not a very large source of error.

3.2 Comparison of Boundary Conditions: Avalanche Source vs. Mass-momentum Source

The inflow hydrographs of the two boundary condition methods are shown in Fig. 5 along with the hydrograph from the RAMMS avalanche model (Somos-Valenzuela et al., 2016). For all three avalanche scenarios, the peak inflow for the avalanche source was significantly higher than for the mass-momentum source. The mass-momentum boundary condition inflows were very close to those of the RAMMS model in each case because the boundary condition was defined to match the RAMMS avalanche hydrograph. The higher peak inflows for the avalanche boundary condition are probably because the lower viscosity of water relative to the avalanche material allows the fluid to flow and spread out more quickly; to compensate for this, the avalanche boundary condition fluid release volume was concentrated over a smaller area so that the fluid depths would not be too low, but the result was higher inflow rates over a shorter period. The peak inflow rates for the avalanche boundary condition ranged from nearly twice the peak flow rate of the RAMMS avalanche for the large scenario to over 5 times higher for the small scenario, but the inflows for the avalanche boundary condition were of much shorter duration. For the large scenario, peak overtopping discharge for the mass-momentum boundary condition (Table 2) was 14% less than the discharge for the avalanche boundary condition (compared to a difference of about 50% for the inflows). However, for the medium and small scenarios, the difference in peak overtopping discharge between the two boundary

condition models was more pronounced. For the medium mass-momentum boundary condition, the overtopping discharge was 65% less than the discharge from the medium avalanche boundary condition; this difference was only slightly lower than the difference in peak inflow (~75%). The overtopping discharge for the small mass-momentum boundary condition was almost 91% less than the discharge for the small avalanche boundary condition (with difference in peak inflow of around 80%). While the difference in overtopping volumes for the *large* avalanche and mass-momentum boundary condition was only 9%, the total overtopping volume for the *small* mass-momentum boundary condition was over an order of magnitude less than the overtopping volume resulting from the small avalanche boundary condition (Table 2).

There were a few irregularities in the inflow hydrographs that should be mentioned. First, the large avalanche source inflow hydrograph had a bimodal peak, likely due to the way in which the initial avalanche fluid volume was defined. The initial fluid volume was defined as blocks of water above the natural terrain, the surface elevations of which were set at graduated levels, taking the shape of steps to more closely mimic the natural descent of the terrain and have a relatively constant initial water depth; this definition of the initial fluid release volume is not realistic, but after it was released, the fluid flowed into a more natural state. However, for the large avalanche source, the sections of the initial fluid volume most likely had variations in the initial water surface elevation that were too abrupt so that the fluid did not coalesce into one continuous surface but rather had two areas of peak flow depth. This is a problem that results from releasing blocks of water just above the lake; the initial fluid volume is not realistic, but water will even out into a natural flow before it reaches the lake. The fluid cannot be released at a point that is too high or the velocities will be excessive, but to get a high enough volume with accurate depths, it is difficult to get an even flow by the time the water reaches the lake. A second irregularity was the smaller, second peak in the inflow hydrographs from the avalanche boundary condition in the medium and small scenarios, likely the result of flow entering the lake from the sides. This is not unrealistic, since there was inflow from the sides of the lake in the avalanche model. However, due to the higher viscosity of the snow-rock-ice mixture of the avalanche, the inflow from the lateral moraines probably would happen more gradually so that the abrupt inflow from the sides would not cause such a significant peak in the inflow hydrograph.

3.3 Wave Characteristics

The impact of the avalanche with the lake generates a large tsunami-like wave. As the wave propagates across the lake, it reaches a maximum height as it approaches the shallow part of the lake near the damming-moraine (Fig. 6). The characteristics of the waves generated for each avalanche scenario are given in Table 3. The FLOW 3D wave heights were all larger than the empirically-calculated wave heights (Heller and Hager, 2010); however, the waves were of a similar magnitude with both methods with a difference in maximum wave height between FLOW 3D and the empirical method of 14% (5.8 m) for the large avalanche source. The FLOW 3D results showed attenuation of the wave as it propagated along the lake; this attenuation resulted in a reduction in the wave height of approximately 30% before the wave began the run-up phase (Fig. 6).

Upon closer examination, the wave generated from the large avalanche source (Fig. 6) had two peaks that were of similar height. The first peak was near the avalanche impact, corresponding to the location of the wave represented

by the empirical equations; the second peak, that was slightly higher, occurred as the wave began to run up on the shallower part of the lake. The wave characteristics calculated by the empirical method consider the wave generation process but do not account for the impact of run-up on the wave characteristics. Therefore, the peak wave height in the deeper portion of the lake is the closest point of comparison with the empirical equations. Fig. 6 gives the wave height as a function of distance along the lake (not as a function of time); there were some oscillations in the profile of the maximum wave height, most likely due to splashing from the run-up on the sides that was reflected off the lateral moraines and returned to the lake at irregular intervals.

3.4 Overtopping Hydrographs and Volumes

The run-up phase culminates with the moraine overtopping; the wave heights given in Table 2 correspond to the height above the moraine crest as the wave overtops the damming-moraine. The volume of water that resulted from the overtopping of the moraine was significant; the total overtopping discharge volume for each scenario is given in Table 2, and the overtopping hydrographs are shown in Fig. 7. The large avalanche source resulted in a peak overtopping discharge of approximately 63,000 m^3/s that occurred around 60 s after the start of the avalanche as well as a smaller peak of 6,000 m^3/s resulting from the overtopping of the reflected wave. The overtopping of the initial wave lasted about 100 seconds for the large avalanche source, 70 seconds for the medium avalanche source, and 50 seconds for the small avalanche source.

The mass-momentum boundary condition consistently resulted in lower overtopping discharges and volumes, but the differences between the mass-momentum and avalanche boundary condition were more pronounced for the small and medium scenarios. For the large mass-momentum boundary condition, the peak overtopping flow rate was 14% less than that of the avalanche boundary condition. The large mass-momentum boundary condition overtopping volume was 11% less than the avalanche boundary condition overtopping volume. For the medium mass-momentum boundary condition, the peak discharge and overtopping volume were 65% and 70% less than the avalanche boundary condition, respectively, and the difference in both the peak discharge and overtopping volume between the small avalanche and mass-momentum boundary conditions was 91%.

The overtopping volumes for all scenarios were less than the volume of avalanche material entering the lake. The overtopping volume for the large avalanche boundary condition was 60% of the avalanche volume, and for the medium and small avalanche boundary conditions, the overtopping volumes were 50% and 30% of the avalanche volumes respectively. The overtopping volume decreases relative to the avalanche volume as the avalanche size decreases, indicating that the lake has more capacity to dissipate smaller avalanche-generated waves.

3.5 Lake Lowering Scenarios

Two scenarios of lake lowering were simulated to evaluate the potential effect of lowering the lake level as a mitigation strategy. Three avalanche sizes and both types of boundary conditions were simulated with each lake level, resulting in a total of 18 simulations. The overtopping volumes and peak discharges were somewhat reduced by lowering the lake 15 m, while 30 m lowering resulted in even further reductions in overtopping discharges (Table 2). The hydrographs for the overtopping discharge are shown in Fig. 8.

Lowering the lake level, even by as much as 30 m, did not completely prevent overtopping of the damming-moraine. Nonetheless, overtopping may be prevented by lake lowering for smaller avalanches. A 90% reduction of overtopping volume may be achieved for the medium avalanche boundary condition through lowering the lake level by 30 m. Overtopping was not avoided entirely with the 15 m lake lowering, but the overtopping volumes and discharges were approximately 60% and 80% less than with the current lake level for the medium and small avalanches, respectively. Lake lowering appears to have the least impact for large avalanches, as significant overtopping still occurred under all lake lowering scenarios for a large avalanche. However, the overtopping volume was reduced by 28% for the large avalanche boundary condition, with 30 m lake lowering and by 73% for the large mass-momentum boundary condition, with 30 m lake lowering. The categorization of each scenario according to the definition of a "safe scenario" (Sect. 2.4) is given in Table 4.

The overtopping wave heights increased with lake lowering even though the total overtopping volumes and peak flow rates decreased. The total volume in the lake decreased with lake lowering, and the avalanched impacted the lake at a lower elevation; the ratio of the momentum relative to the lake volume increased with lake lowering, thus generating higher waves. Although the increased overtopping wave heights with lake lowering indicates that the waves may be larger when the lake is lowered, the amount of overtopping is still reduced. The lower initial water surface elevation means that more momentum is required for overtopping, since more momentum is lost during run-up and overtopping, less water is able to pass over the crest of the terminal moraine.

4 Discussion

This paper presents three-dimensional simulations of avalanche-generated waves, one step in the GLOF chain of processes. The lake hydrodynamic model improves upon previous two-dimensional SWE simulations of avalanche-generated waves in GLOF process chain modeling that must be calibrated with data from past GLOF events (e.g., Schneider et al., 2014). Many glacial lakes that are currently dangerous have not previously outburst, so the use of data from prior GLOF events is not an option at many study sites. Additionally, GLOF modeling for hazard mapping requires predictive modeling of multiple scenarios. Because three-dimensional non-hydrostatic models represent more of the physical processes, they require less calibration and can be used for predictive modeling of lake dynamics and moraine overtopping. Thus, three-dimensional lake models may be a desirable alternative to two-dimensional SWE models for wave simulations. Despite the advantages of three-dimensional models for hydrodynamic lake simulations, these models still carry a considerable amount of uncertainty, and there is a dearth of field observations that can be used for model validation.

Although the avalanche boundary condition seems to have more uncertainty than the mass-momentum boundary condition, each boundary condition method has its limitations. The complex nature of the interacting dynamic physical systems makes it difficult to develop a comprehensive and precise method for simulating avalanche-generated waves in glacial lakes. Avalanches typically consist of a mixture of snow, ice and rock, and the biggest limitation of the boundary conditions in this model is the representation of the avalanche fluid as water because the dissipation of energy of the actual avalanche material is different from water. This limitation can be partially overcome by calibrating the model to replicate the depth and velocity characteristics of the avalanche as it enters the

lake. This is done by adjusting the avalanche release area in the avalanche boundary condition and the hydrograph and cross-sectional area of the inflow for the mass-momentum boundary condition. However, it is impossible to completely replicate the avalanche characteristics in the lake hydrodynamic model, and there are significant differences in the inflow hydrographs of the FLOW 3D model and the RAMMS avalanche model (like the mass-momentum source) when the avalanche boundary condition is used. The discrepancies between the avalanche and mass-momentum boundary conditions are more pronounced for smaller avalanches, but there is no obvious solution to overcome this difficulty when using the avalanche boundary condition. To further advance the simulation of avalanche-generated waves, models are needed that can easily and accurately represent two distinct fluids (in this case the mixture of snow, rock and ice of the avalanche and the water in the lake) combined with free surface flows. Without two-phase models that can simulate free surface flows, it will not be easy to overcome the limitations and irregularities of the model that result from the representation of the avalanche fluid as water.

The avalanche boundary condition has much higher and possibly unrealistic peak inflow rates, but it gives a better physical representation of the actual geometry of the terrain as the avalanche enters the lake. The avalanche boundary condition is also able to simulate the effects of avalanche material entering the sides of lake, whereas the mass-momentum boundary condition only simulates flow entering from the end of the lake. The mass-momentum boundary condition better matches the peak flow rates of the avalanche because that is how the method was designed; the flow rate of the avalanche inflow is a control parameter for the mass-momentum boundary condition. However, under this boundary condition, the avalanche material enters the lake horizontally, rather than on the steep incline of the actual terrain above the lake. Therefore, this boundary condition likely underestimates the momentum transfer between the avalanche and the lake, as the avalanche can gain more momentum as it enters the lake at a downward angle. Despite the limitations of each boundary condition method, they are representing a range of possible outcomes, and the results could be considered as upper and lower bounds on the overtopping discharge from the lake model. Because we do not have any field measurements of the characteristics of avalanche-generated waves during GLOF events or the resulting discharge hydrographs, we do not possess the means of validating the model results presented in this paper or conclusively evaluating the boundary condition methods.

The avalanche simulation is the process in the GLOF chain of events that carries the greatest uncertainty because avalanche dynamics may be the least understood of the processes. The range of uncertainty in the avalanche conditions (depths, flow rates and velocities) is possibly greater than the range of variability in the inflow hydrographs for the lake model. We have no estimates of the uncertainty in the avalanche model, but any uncertainties in the avalanche simulations are propagated into the lake model and subsequent processes in the GLOF chain of events. Although there is significant variability between the avalanche and mass-momentum boundary condition results, the range of variability in the peak flow and shape of the avalanche hydrographs may be even greater than the variability in the discharge hydrographs from the lake model.

The characteristics of the wave as it propagates across the lake are significant indicators of the magnitude of the event that is being simulated. The wave heights are quite large (up to nearly 50 m tall) when compared with the initial depths of the lake that range from 72 m to less than 10 m. Such large waves relative to the lake depths indicate that vertical accelerations are significant and should not be neglected. Thus, a non-hydrostatic model is

essential for accurately representing the wave dynamics. Wave heights from the FLOW 3D simulations were compared with those calculated with the empirical equations. The FLOW 3D simulations reproduced the characteristics of the RAMMS avalanche as it impacted the lake while also accounting for lake bathymetry; thus, the FLOW 3D model can likely produce more realistic wave characteristics than the empirical method. For the large avalanche scenario, both boundary conditions resulted in wave heights that were only 4.4-5.8 m higher than the empirically calculated wave heights. However, it is worth noting that the maximum wave height for the large avalanche boundary condition occurred at the beginning of the run-up phase in the shallow part of the lake, and the first wave peak in the deep portion of the lake was closer to the empirically predicted height. The large differences between the empirical and FLOW 3D wave heights for the medium and small scenarios may be due to the shortcomings of the avalanche boundary condition. Nevertheless, the relatively close agreement between the empirical and hydrodynamic models for the large avalanche scenario indicates that it may be possible to use the empirical method as a calibration tool.

During the run-up phase of the wave propagation, two things happened simultaneously. The wave height increased somewhat due to the run-up in the shallow portion of the lake, but there was also some energy loss due to the sharp discontinuity in the lakebed geometry. Generally, one might expect the wave height to increase even more than what occurred in the FLOW 3D simulations; however, due to the lakebed geometry, there is more dissipation of energy when the wave reaches the shallow portion of the lake than would occur if there were a more gradual transition between the deep and shallow areas of the lake.

The greatest uncertainty in the lake modeling arises from the wave generation and avalanche characteristics. Uncertainties due to the turbulence model and grid size are not negligible, but they are small compared to the magnitude of uncertainty from the wave generation. One way to estimate the uncertainty in the wave generation is by using more than one method to represent the impact of the avalanche with the lake (i.e., the two methods for modeling the boundary conditions). Without any in situ data from real events, the level of uncertainty cannot be estimated precisely, but given the range of overtopping flows and volumes from the two boundary condition methods, the uncertainty is considerable. Although there is no way to validate the results to know which type of boundary condition is more representative of the actual conditions, it is possible that the avalanche boundary condition is overestimating the momentum transfer while the mass-momentum boundary condition is likely underestimating it. The avalanche boundary condition could represent an upper bound for the simulation results while the mass-momentum source may be closer to a lower bound.

This paper focuses exclusively on the lake hydrodynamics and does not consider the question of dynamic erosion of the terminal moraine due to overtopping flows. The potential erosion of the terminal moraine is an important factor to consider when assessing the hazard level of any glacial lake with a moraine dam. For Lake Palcacocha, this was assessed by Somos-Valenzuela et al. (2016) through a separate hydromorphodynamic model, and the conclusion was that despite significant potential for erosion, the moraine is extremely unlikely to fail.

The results from the large avalanche simulations represent the worst-case scenario of an avalanche-induced GLOF from Lake Palcacocha if the moraine is as stable as it seems. Given the significant differences between the small and medium avalanche simulations, results from both boundary condition methods should be provided if these scenarios

and their likelihoods will be used in an economic or risk and vulnerability analysis of the mitigation alternatives. All the large avalanche scenarios and most of the medium avalanche scenarios resulted in significant overtopping, even with lake lowering. However, the definition of a "safe scenario" used here is not fully indicative of the effect of lake lowering on hazard mitigation. The downstream impacts for each scenario should be considered when evaluating lake lowering scenarios. The possible reduction in inundated area and flood intensity zones for the lake lowering scenarios are discussed in Somos-Valenzuela et al. (2016). The potential for lake lowering works to prevent overtopping for the small and medium avalanche scenarios is significant because small and medium avalanches are believed to be much more likely than large avalanches; therefore, the real impact of lake lowering may be more than is immediately apparent with these results. However, from the modeling results alone it is not possible to determine an optimum lake level. Further economic and vulnerability analyses are necessary to recommend an ideal mitigation alternative.

5 Conclusions

Improving the understanding of lake dynamics during GLOF events requires using three-dimensional non-hydrostatic models to simulate avalanche-generated waves. The simulations of Lake Palcacocha show that waves of considerable magnitude can be produced. The avalanche characteristics and the shape of the inflow hydrographs substantially influence the overtopping wave volumes. The results indicate that large avalanches pose the greatest threat to the city of Huaraz, but even smaller avalanches could generate significant overtopping discharges, resulting in substantial inundation in the city. Lowering the lake level may reduce the overtopping volume and discharge for a large avalanche, but it is not possible to eliminate the potential for overtopping. For small and medium avalanches, it may be possible for the wave to be contained in the lake if the water surface is lowered. However, given the range of uncertainty in the model results, it cannot be stated conclusively that lowering the lake level would prevent overtopping for smaller avalanches. Even though the precise reduction in hazard level due to lake lowering cannot be quantified, it is reasonable to conclude that lowering the level of Lake Palcacocha can reduce the hazard levels in the city of Huaraz.

The modeling reported here provides a significant advancement beyond previous simulations of avalanche-generated waves. Model calibration is less important for the three-dimensional modeling approach due to the improved representation of physical processes as compared with two-dimensional SWE models; therefore, it presents an alternative that can be used when field data from a prior GLOF are not available for model calibration. Despite the advantages of this method, uncertainties are still present; however, as the fundamental physical phenomena are better represented in three-dimensional models, errors can be attributed more to uncertainties in the physical parameters, initial and boundary conditions rather than the model constructs. Nonetheless, the lake dynamics still remain a problematic link in attempts to model the GLOF process chain.

Avalanche simulation is the GLOF process chain link that carries the greatest uncertainty, and much of that is propagated into the lake model. Precise knowledge of avalanche behavior is limited, and so it is difficult to evaluate how well the lake model represents the avalanche as it enters the lake. Because the lake model is so heavily influenced by the avalanche characteristics, it is difficult to quantify the uncertainty in the wave simulations. More

studies are needed to gain a better understanding of the magnitudes and sources of uncertainty in glacial lake modeling of waves generated by mass movements.

Competing Interests

The authors declare that they have no conflict of interest.

Acknowledgements

The USAID Climate Change Resilient Development (CCRD) and Sustaining Mountain and Water Livelihoods (SMWL) projects have provided support that made this work possible. The authors would like to thank the software developers from Flow Science, Inc. for the FLOW 3D license and technical assistance. Marcelo Somos-Valenzuela, Denny Rivas, and Cesar Portocarrero were indispensable resources who gave helpful feedback and encouragement. The authors are very grateful for the constructive comments of the anonymous reviewers.

References

Abadie, S., Morichon, D., Grilli, S., Glockner, S. Numerical simulation of waves generated by landslides using a multiple-fluid Navier–Stokes model. Coast. Eng., 57, 779–94, 2010.

Allen, S. K., Linsbauer, A., Randhawa, S. S., Huggel, C., Rana, P., Kumari, A. Glacial lake outburst flood risk in Himachal Pradesh, India: an integrative and anticipatory approach considering current and future threats. Nat. Hazards, 84, 1741-1763, 2016. DOI 10.1007/s11069-016-2511-x

ANA – Autoridad Nacional del Agua. Informe Tecnico Colegiado sobre las Acciones, Actividades, y Proyectos Que Deben Ejecutarse, Para Disminuir el Riesgo de Desastre por Desembalse de la Laguna Palcacocha (Huaraz – Ancash). *Autoridad Nacional del Agua, Instituto Geofísico del Peru, Instituto Geológico Minero y Metalúrgico, Instituto Nacional de Defensa Civil, Centro Nacional de Estimación Prevención y Reducción de Riesgos de Desastres*. Huaraz, Peru, 2013.

Ataie-Ashtiani, B., Yavari-Ramshe, S. Numerical simulation of wave generated by landslide incidents in dam reservoirs. Landslides. 8(4), 417-432, 2011.

Awal, R., Nakagawa, H., Fujita, M. K., Baba, Y., & Zhang, H. Experimental study on Glacial Lake Outburst Floods due to waves overtopping and erosion of moraine dam. Annuals of Disas. Prev. Res Inst., Kyoto University, *53B*, 583-594, 2010.

Bajracharya, B., Shrestha, A. B., Rajbhandari, L. Glacial Lake Outburst Floods in the Sagarmatha Region: Hazard assessment using GIS and Hydrodynamic Modeling. Mt. Res. Dev. 27(4), 336-344, 2007.

Bartelt, P., Buehler, Y., Christen, M., Deubelbeiss, Y., Salz, M., Schneider, M., Schumacher, L. RAMMS: Rapid Mass Movement Simulation: A numerical model for snow avalanches in research and practice. User Manual v1.5 – Avalanche. Swiss Federal Institute for Forest, Snow and Landscape Research WSL. Birmensdorf. 89 pp, 2013.

Benn, D. I. Evans, D. J. A.: Glaciers and Glaciation. Second Edition, Hodder Education. London. 2010.

Biscarini, C. Computational Fluid Dynamics Modelling of Landslide Generated Water Waves. Landslides, 7, 117-124, 2010.

Capel, A. Wave run-up and overtopping reduction by block revetments with enhanced roughness. Coast. Eng., 104, 76-92, 2015. DOI: 10.1016/j.coastaleng.2015.06.007

Carey, M. In the Shadow of Melting Glaciers: Climate Change and Andean Society. New York: Oxford Univ. Press. 288 pp., 2010.

Carey, M., Huggel, C., Bury, J., Portocarrero, C., Haeberli, W. An integrated socio-environmental framework for glacier hazard management and climate change adaptation: lessons from Lake 513, Cordillera Blanca, Peru. Climatic Change. 112, 733-767, 2012. DOI: 10.1007/s10584-011-0249-8

Christen, M., Kowalski, J., Bartelt, P. RAMMS: numerical simulation of dense snow avalanches in three-dimensional terrain. Cold Reg. Science and Technol., 63, 1–14, 2010.

Clague, J. J., Evans, S. G. A Review of Catastrophic Drainage of Moraine-Dammed Lakes in British Columbia. Quaternary Sci. Rev., 19, 1763–1783, 2000.

Cook, S. J., Kougkoulos, I., Edwards, L. A., Dortch J., Hoffmann, D. Glacier change and glacial lake outburst flood risk in the Bolivian Andes. Cryosphere. 10, 2399–2413, 2016. doi:10.5194/tc-10-2399-2016

Costa, J. E., Schuster, R. L. The formation and failure of natural dams. Geol. Soc. Am. Bull., 100, 1054-1068, 1988.

Cremonesi, M., Frangi, A., Perego, U. A Lagrangian finite element approach for the simulation of water-waves induced by landslides. Comput. Struct., 89**:**1086–93, 2011.

Dean, R. G., Dalrymple, R. A. Water wave mechanics for engineers and scientists. Singapore: World Scientific, 1991.

Diario La Republica. Declaran en emergencia la laguna Palcacocha en Huaraz. La republica. 2010. Retrieved from http://larepublica.pe/20-04-2010/declaran-en-emergencia-la-laguna-palcacocha-en-huaraz. Accessed on October 14, 2016.

Emmer, A., Cochachin, A. Causes and mechanisms of moraine- dammed lake failures in Cordillera Blanca (Peru), North American Cordillera and Central Asia, AUC Geographica, 48(2), 5-15, 2013.

Emmer, A., Vilimek, V. Review Article: Lake and breach hazard assessment for moraine-dammed lakes: an example from the Cordillera Blanca (Peru). Nat. Hazard Earth Sys., 13(6), 1551-1565, 2013.

Emmer, A., Vilímek, V. New method for assessing the susceptibility of glacial lakes to outburst floods in the Cordillera Blanca, Peru. Hydrol. Earth Syst. Sci., 18, 3461–3479, 2014.

Emmer, A., Vilímek, V., Huggel, C., Klimes, J., Schaub, Y. Limits and challenges to compiling and developing a database of glacial lake outburst floods. Landslides. 13(6), 1579-1584, 2016a. DOI: 10.1007/s10346-016-0686-6

Emmer, A., Vilímek, V., Zapata, M. L. Hazard mitigation of glacial lake outburst floods in the Cordillera Blanca (Peru): the effectiveness of remedial works. Journal of Flood Risk Management, 13 pp., 2016b. DOI: 10.1111/jfr3.12241

Espinoza, E. S. Identificación de los Riesgos Relacionados con la Laguna Palcacocha. Institución en Clima para la Accion (INCLIMA). Lima, Peru, 2013.

Etemad-Shahidi, A., Shaeri, S., Jafari, E. Prediction of wave overtopping at vertical structures. Coast. Eng., 109, 45-52, 2016. DOI: 10.1016/j.coastaleng.2015.12.001

Fah, R. Numerik an der VAW: Entwicklungen und Beispiel des Triftgletschers, In: Festkolloquium VAW 75 JAHRE, edited by: Minor, H.-E., Versuchsanstalt für Wasserbau, Hydrologie und Glaziologie ETH-Zentrum CH-8092 Zürich, 187–200, 2005.

Flow Science. FLOW-3D Documentation: Release 10.1.0, Flow Science, Inc. Santa Fe, NM, 2012.

Fritz, H. M., Hager, W. H., Minor, H. E. Near Field Characteristics of Landslide Generated Impulse Waves. J. Waterw. Port C-ASCE, 130, 287-302, 2004.

Ghozlani, B., Hafsia, Z., Maalel, K. Numerical study of surface water waves generated by mass movement. *Fluid Dyn. Res.*, 45(5), Article Number: 055506, 2013.

Haeberli, W., Alean, J.-C., Müeller, P., Funk, M. Assessing Risks from Glacier Hazards in High Mountain Regions: Some Experiences in the Swiss Alps. Ann. Glaciol., 13, 96–102, 1989.

Heinrich, P. Nonlinear Water Waves Generated by Submarine and Aerial Landslides. J. Waterw. Port C-ASCE, 118, 249-266, 1992.

Heller, V., Hager, W. H. Impulse Product Parameter in Landslide Generated Impulse Waves. J. Waterw. Port C-ASCE, 136, 145-155, 2010.

Heller, V., Bruggemann, M., Spinneken, J., Rogers, B. Composite modelling of subaerial landslide–tsunamis in different water body geometries and novel insight into slide and wave kinematics. Coast. Eng., 109, 20-41, 2016.

Huggel, C., Haeberli, W., Kaäb, A., Bieri, D., Richardson, S. An assessment procedure for glacial hazards in the Swiss Alps, Canadian Geotech. J., 41, 1068–1083, 2004.

INDECI – Instituto Nacional de Defensa Civil. Informe de peligro Nº 003-12/05/2011/COEN-SINADECI/ 15:00 horas (Informe Nº 01): Peligro por aluvión en el departamento de Ancash. Huaraz-Peru: COEN-SINADECI, 2011.

INDECI – Instituto Nacional de Defensa Civil. Laguna Palcacocha y su Impacto en los Distritos de Huaraz e Independencia, en Caso de Desborde y Probable Aluvión Departamento de Ancash. Dirección de Preparación-CEPIG. Lima, Peru, 2015.

INEI – Instituto Nacional de Estadística e Informática. Censos Nacionales de Población y Vivienda: XI de Poblacion y VI de Vivienda. Instituto Nacional de Estadística e Informática, Presidencia del Consejo de Ministros de Peru. 2007.

Isfahani, A. H. G., Brethour, J. M. On the Implementation of Two-equation Turbulence Models in FLOW-3D. Flow Science, Inc. Santa Fe, NM, 2009.

Kafle, J., Pokhrel, P. R., Khattri, K. B., Kattel, P., Tuladhar, B. M., Pudasain, S. P. Landslide-generated tsunami and particle transport in mountain lakes and reservoirs. Ann. Glaciol., *57*(71), doi: 10.3189/2016AoG71A034, 2016.

Kamphuis, J.W., Bowering, R.J. Impulse waves generated by landslides. Proc. 12th Coastal Engineering Conf., ASCE, *1*, 575-588, 1970.

Klimes, J., Benesová, M., Vilímek, V., Bouska, P., Cochachin-Rapre, A. HEC-RAS and its significance for future hazard assessments: an example from Lake 513 in the Cordillera Blanca, Peru. Nat. Hazards, 71(3), 1617-1638, 2014.

Linsbauer, A. Frey, H., Haeberli, W., Machguth, H., Azam, M. F., Allen, S. Modelling glacier-bed overdeepenings and possible future lakes for the glaciers in the Himalaya–Karakoram region. Ann. Glaciol. 57(71):119-130, 2016. doi: 10.3189/2016AoG71A627.

Liu, P. L.-F., Wu, T.-R., Raichlen, F., Synolakis, C. E., Borrero, J. C. Runup and rundown generated by three-dimensional sliding masses. J. Fluid Mech., 536, 107–44, 2005.

Lliboutry, L., Morales Arnao, B., Pautre, A., Schneider, B. Glaciological problems set by the control of dangerous glacial lakes in Cordillera Blanca, Peru. I. Historical failures of morainic dams, their causes and prevention. J. Glaciol., 18(79), 239-254, 1977.

Muller, D.R. Auflaufen and Uberschwappen von Impulswellen an Talsperren: Zurich, VAW- ETH, Mitt. Nr. 137., 1995.

Pope, S. B. Turbulent Flows. Cambridge: Cambridge UP. 771 pp., 2000.

Portocarerro, C. Reducing Risk from Dangerous Glacial Lakes in the Cordillera Blanca, Peru, Technical Report: The Glacial Lake Handbook. High Mountains Adaptation Program, United States Agency for International Development, Washington D.C., 2014.

Reynolds, J. M. Development of glacial hazard and risk minimisation protocols in rural environments, Methods of glacial hazard assessment and management in the Cordillera Blanca, Peru. Reynolds Geo-Sciences Ltd., Flintshire (UK), 72 pp., 2003.

Richardson, S. D., Reynolds, J. M. An Overview of Glacial Hazards in the Himalayas. Quatern. Int., *65–66*, 31–47, 2000.

Rivas, D. S., Somos-Valenzuela, M. A., Hodges, B. R., McKinney, D. C. Predicting outflow induced by moraine failure in glacial lakes: The Lake Palcacocha case from an uncertainty perspective. Nat. Hazards Earth Syst. Sci., *15*, 1163-1179, 2015.

Romano, A., Bellotti, G., Briganti, R., & Franco, L. Uncertainties in the physical modelling of the wave overtopping over a rubble mound breakwater: The role of the seeding number and of the test duration. Coast. Eng., 103, 15-21, 2015. DOI: 10.1016/j.coastaleng.2015.05.005

Rounce, D. R., McKinney, D. C., Lala, J. M., Byers, A. C., Watson, C. S. A new remote hazard and risk assessment framework for glacial lakes in the Nepal Himalaya. Hydrol. Earth Sys. Sci., 20, 3455-3475, 2016.

Rzadkiewicz, S.A., Mariotti, C., Heinrich, P. Numerical Simulation of Submarine Landslides and their Hydraulic Effects. J. Waterw. Port C-ASCE, 123, 149-157, 1997.

Schneider, D., Huggel, C., Cochachin, A., Guillén, S., García, J. Mapping hazards from glacier lake outburst floods based on modelling of process cascades at Lake 513, Carhuaz, Peru. Adv. Geosci., 35, 145–155, 2014.

Schwanghart, W., Worni, R., Huggel, C., Stoffel, M., Korup, O. Uncertainty in the Himalayan energy–water nexus: estimating regional exposure to glacial lake outburst floods. Environ. Res. Lett., 11, 074005, 2016. doi:10.1088/1748-9326/11/7/074005

Slingerland, R. L., Voight, B. Occurences, Properties and Predictive Models of Landslide-generated Impulse Waves. Rockslides and Avalanches, 2, 317-397, Ed. Voight, B. Developments in Geotechnical Engineering, 14B. Elsevier, Amsterdam, 1979.

Slingerland, R. L., Voight, B. Evaluating hazard of landslide-induced water waves. J. Waterw. Port C-ASCE, 108(WW4), 504-512, 1982.

Somos-Valenzuela, M. A., Chisolm, R. E., Rivas, D. S., Portocarrero, C., McKinney, D. C.: Modeling glacial lake outburst flood process chain: the case of Lake Palcacocha and Huaraz, Peru, Hydrol. Earth Syst. Sci., 20, 2519–2543, 2016. doi: 10.5194/hess-20-2519-2016

Synolakis, C. E. The runup of solitary waves. J. Fluid Mech., 185, 523-545, 1987.

Synolakis, C. E. Tsunami runup on steep slopes—How good linear theory really is. Nat. Hazards, 4, 221-234, 1991.

UGRH – Unidad de Glaciologia y Recursos Hídricos. Bathymetric survey of Lake Palcacocha. Autoridad Nacional de Agua (ANA) de Perú, Huaraz, Peru, 2009.

UGRH – Unidad de Glaciologia y Recursos Hídricos. Inventario de lagunas glaciares del Peru. Inventario nacional de glaciares y lagunas. Autoridad Nacional del Agua, Direccion de Conservacion y Planeamiento de Recursos Hidricos, Huaraz, Peru, 2014.

UGRH – Unidad de Glaciologia y Recursos Hídricos. Bathymetric survey of Lake Palcacocha. Autoridad Nacional de Agua (ANA) de Peru, Huaraz, Perú, 2016.

Valderrama, P., Vilca, O. Dinamica e implicaciones del aluvión de la Laguna 513, Cordillera Blanca, Ancash Perú. Revista de la Asociación Geológica Argentina. 69(3), 400-406, 2012.

Valderrama, P., Pari, W., Silva, C., Fídel, L. Evaluación Ingeniero – Geológico: Laguna de Palcacocha y su Influencia en la Ciudad de Huaraz Cordillera Blanca. Informe Técnico No. A6631. Instituto Geológico Minero y Metalúrgico (INGEMMET), Sector Energía y Minas. Ancash, Peru, 2013.

Vilimek, V., Zapata, M. L., Klimes, J., Patzelt, Z., Santillan, N. Influence of glacial retreat on natural hazards of the Palcacocha Lake area, Peru, Landslides, 2, 107–115, 2005.

Wang, W., Yao, T., Gao, Y., Yang, X., & Kattel, D. B. A first–order method to identify potentially dangerous glacial lakes in a region of the southeastern Tibetan Plateau. Mountain Res. Develop., 31, 122–130, 2011.

Wang, W., Gao, Y., Anacona, P. I., Lei, Y., Xiang, Y., Zhang, G., Li, S., Lu, A. Integrated hazard assessment of Cirenmaco glacial lake in Zhangzangbo valley, Central Himalayas. Geomorphology, 2015a. DOI: 10.1016/j.geomorph.2015.08.013

Wang, W., Xiang, Y., Gao, Y., Lu, A., Yao, T. Rapid expansion of glacial lakes caused by climate and glacier retreat in the Central Himalayas. Hydrol. Process., 29, 859–874, 2015b. DOI: 10.1002/hyp.10199

Wang, W., Chen, G., Zhang, H., Zhou, S., Liu, S., Wu, Y., Fu-song Fan, F. Analysis of landslide-generated impulsive waves using a coupled DDA-SPH method. Engineering Analysis with Boundary Elements, 64, 267-277, 2016. DOI: 10.1016/j.enganabound.2015.12.014.

Wegner, S. A. Lo Que el Agua se Llevó: Consecuencias y Lecciones del Aluvión de Huaraz de 1941. Technical Note 7 of the series "Technical Notes on Climate Change", Ministry of Environment, Lima, Peru, 2014.

Westoby, M. J., Glasser, N. F., Brasington, J., Hambrey, M. J., Quincey, D. J., Reynolds, J. M. Modelling outburst floods from moraine-dammed glacial lakes. Earth Science Reviews. 134, 137-159, 2014a. doi: 10.1016/j.earscirev.2014.03.009

Westoby, M. J., Glasser, N. F., Hambrey, M. J., Brasington, J., Reynolds, J. M., Hassan, M. A. A. M. Reconstructing historic Glacial Lake Outburst Floods through numerical modelling and geomorphological assessment: Extreme events in the Himalaya. Earth Surf. Proc. Land., 39(12), 1675-1692, 2014b.

Worni, R., Huggel, C., Clague, J. J., Schaub, Y., Stoffel, M. Coupling glacial lake impact, dam breach, and flood processes: A modeling perspective. Geomorphology, 224, 161–176, 2014.

Yakhot V. & Orszag, S. A. Renormalization group analysis of turbulence. I. Basic theory. J. Sci. Comput., 1, 3-51, 1986.

Zweifel, A., Zuccala, D., Gatti, D. Comparison between Computed and Experimentally Generated Impulse Waves. J. Hydraul. Eng-ASCE, 133, 208-216, 2007.

Table 1. Comparison of overtopping hydrograph characteristics among turbulence models.

#	Model	RMSD (m^3/s)	Difference in Peak Flow Rate		Difference in Overtopping Volume		Difference in Maximum Wave Height	
			m^3/s	%	10^6 m^3	%	m	%
2	RNG-Constant Mixing Length	1,188	-1,100	-1.40	-0.08	-3.60	-0.09	-0.17
3	k-epsilon	726	-2,400	-3.05	-0.11	-4.80	-0.71	-1.38
4	Prandtl Mixing Length	816	-200	-0.25	-0.09	-3.91	0.43	0.83
5	One-Equation-Constant Mixing Length	1,190	-700	-0.89	-0.09	-4.02	0.42	0.80
6	LES	3,047	-6,600	-8.39	-0.25	-10.4	-1.9	-3.64
7	Laminar	3,386	5,200	6.61	0.09	3.60	0.81	1.57

Nat. Hazards Earth Syst. Sci. Discuss., https://doi.org/10.5194/nhess-2017-98
Manuscript under review for journal Nat. Hazards Earth Syst. Sci.
Discussion started: 13 June 2017

Natural Hazards and Earth System Sciences Discussions

Table 2. Overtopping characteristics of three simulated avalanche events of different size for the current lake level and lake lowering scenarios (after Somos-Valenzuela et al., 2016).

Lake lowering	Boundary condition	Overtopping	Avalanche size		
			Large	Medium	Small
Baseline (0 m lower)	Avalanche	Volume (10^6 m^3)	1.80	0.50	0.15
		Peak discharge (m^3/s)	63,400	17,100	6,410
		Wave height (m)	21.7	12.0	7.1
	Mass-momentum	Volume (10^6 m^3)	1.64	0.15	0.014
		Peak discharge (m^3/s)	54,600	6,000	592
		Wave height (m)	15.9	-	-
15 m lower	Avalanche	Volume (10^6 m^3)	1.60	0.20	0.02
		Peak discharge (m^3/s)	60,200	6,370	1,080
		Wave height (m)	38.4	27.5	25.1
	Mass-momentum	Volume (10^6 m^3)	0.83	0.034	0
		Peak discharge (m^3/s)	25,700	1,510	0
		Wave height (m)	32.0	25.4	0
30 m lower	Avalanche	Volume (10^6 m^3)	1.30	0.05	0
		Peak discharge (m^3/s)	48,500	1,840	0
		Wave height (m)	60.8	42.5	0
	Mass-momentum	Volume (10^6 m^3)	0.45	0	0
		Peak discharge (m^3/s)	15,100	0	0
		Wave height (m)	46.1	0	0

Table 3. Comparison of maximum wave heights for FLOW 3D and empirical calculations.

Avalanche size	Boundary condition	Max. wave height (m)		Distance to peak (m)
		Empirical	FLOW 3D	FLOW 3D
Large	Avalanche	42	47.8	1080
	Mass-Momentum		46.4	1039
Medium	Avalanche	21	30.1	318
	Mass-Momentum		NA	NA
Small	Avalanche	9	19.6	108
	Mass-Momentum		NA	NA

Nat. Hazards Earth Syst. Sci. Discuss., https://doi.org/10.5194/nhess-2017-98
Manuscript under review for journal Nat. Hazards Earth Syst. Sci.
Discussion started: 13 June 2017

Natural Hazards and Earth System Sciences
Discussions

Table 4. Characterization of scenario as "safe" or "not safe" according to overtopping criterion.

Avalanche size	Boundary condition	Lake-lowering 0 m	Lake-lowering 15 m	Lake-lowering 30 m
Large	Avalanche	Not Safe	Not Safe	Not Safe
	Mass-momentum	Not Safe	Not Safe	Not Safe
Medium	Avalanche	Not Safe	Not Safe	Not Safe
	Mass-momentum	Not Safe	Not Safe	Safe
Small	Avalanche	Not Safe	Safe	Safe
	Mass-momentum	Safe	Safe	Safe

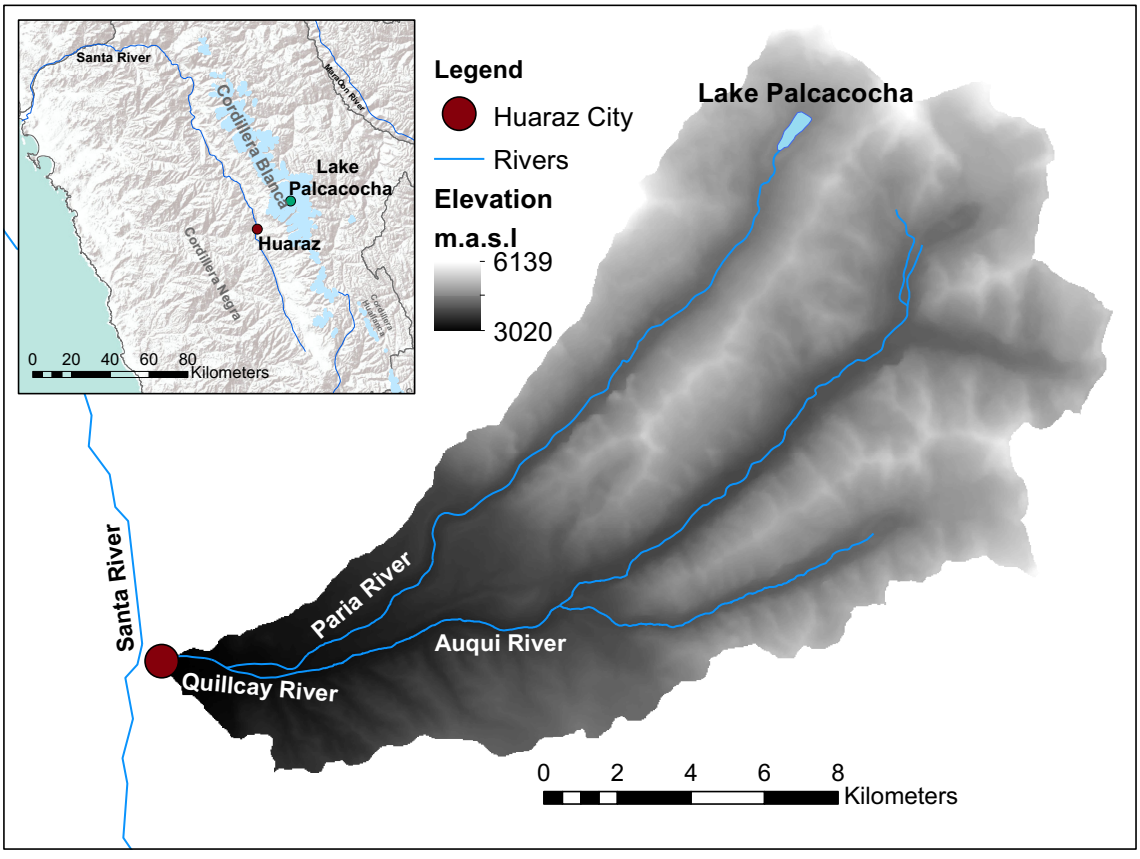

Figure 1: Location of Lake Palcacocha within the Cordillera Blanca, Peru.

Nat. Hazards Earth Syst. Sci. Discuss., https://doi.org/10.5194/nhess-2017-98
Manuscript under review for journal Nat. Hazards Earth Syst. Sci.
Discussion started: 13 June 2017

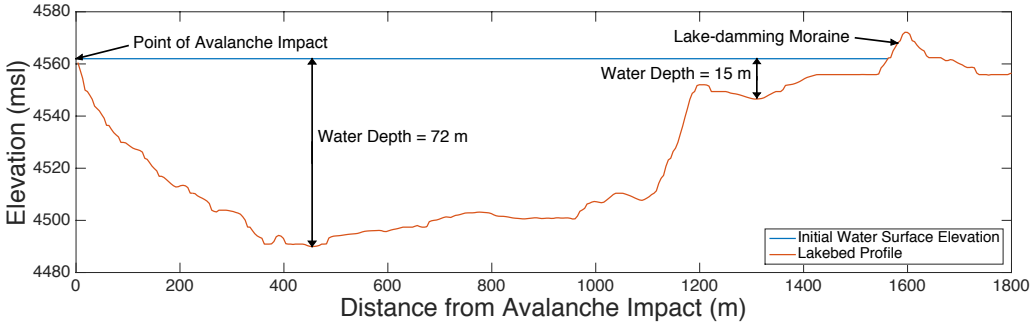

Figure 2. Longitudinal profile of Lake Palcacocha and its terminal moraine.

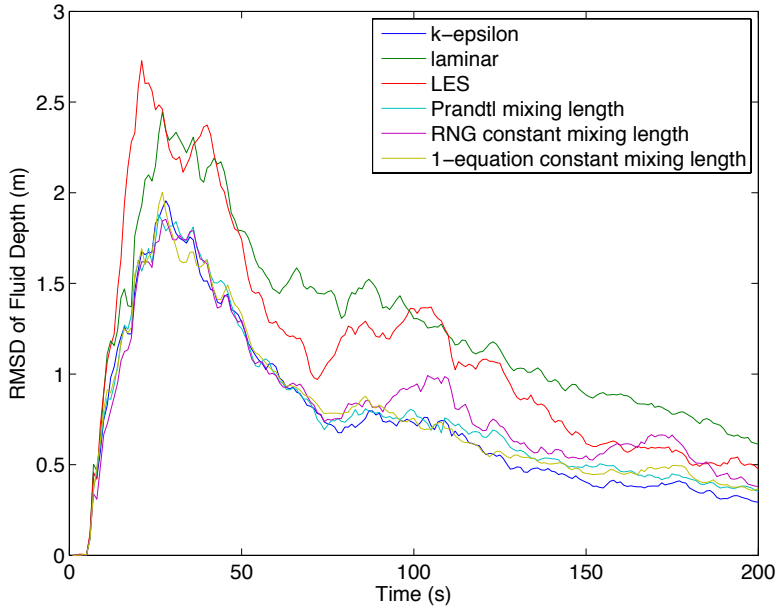

Figure 3. Root-mean-square deviation (RMSD) of fluid depth from the baseline model results (RNG-dynamically computed mixing length) for each turbulence model as a function of time.

Nat. Hazards Earth Syst. Sci. Discuss., https://doi.org/10.5194/nhess-2017-98
Manuscript under review for journal Nat. Hazards Earth Syst. Sci.
Discussion started: 13 June 2017

Natural Hazards and Earth System Sciences
Discussions

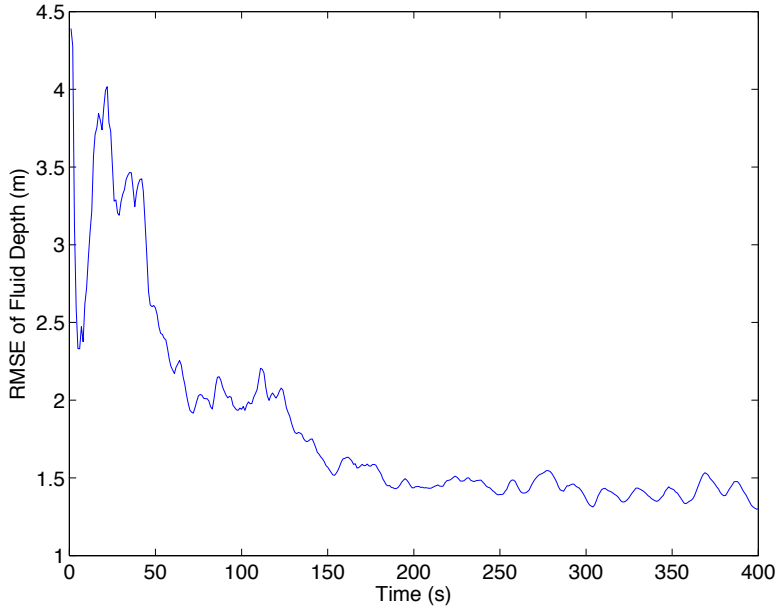

Figure 4. RMSE of fluid depth for the coarse grid simulation as compared to the regular grid mesh using the baseline turbulence model.

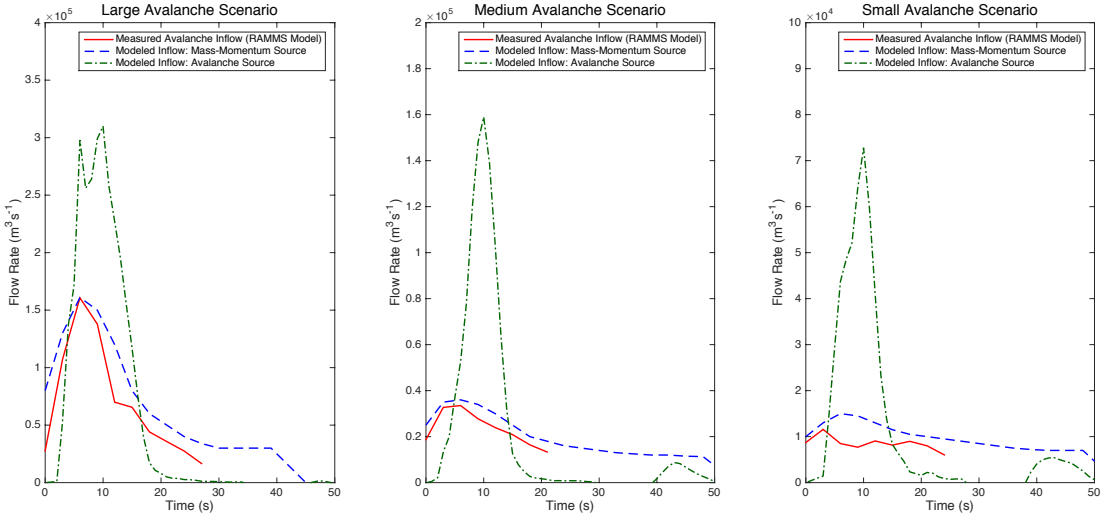

Figure 5. Inflow hydrographs for the avalanche as it enters the lake for the avalanche source and mass-momentum source boundary conditions as compared to the hydrograph extracted from the RAMMS avalanche model.

Nat. Hazards Earth Syst. Sci. Discuss., https://doi.org/10.5194/nhess-2017-98
Manuscript under review for journal Nat. Hazards Earth Syst. Sci.
Discussion started: 13 June 2017

Natural Hazards and Earth System Sciences
Discussions

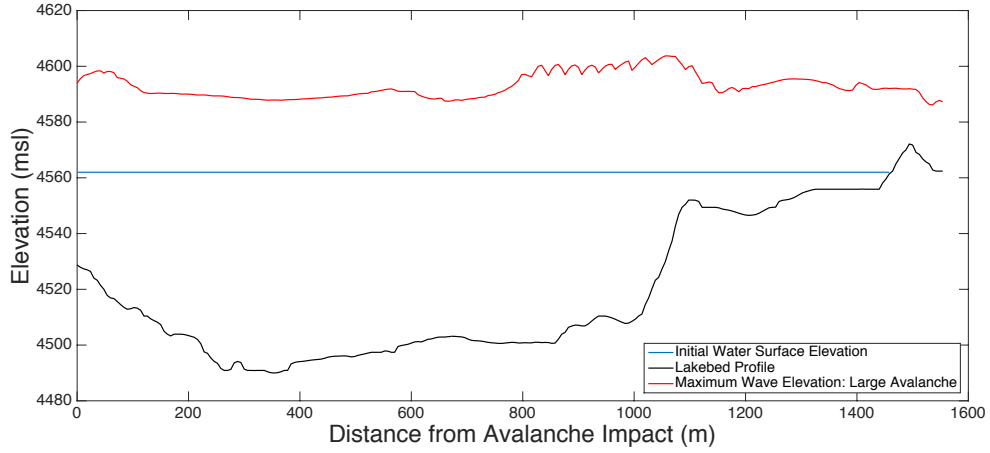

Figure 6. Profile of the maximum wave height as a function of distance along the lake for the large avalanche boundary condition.

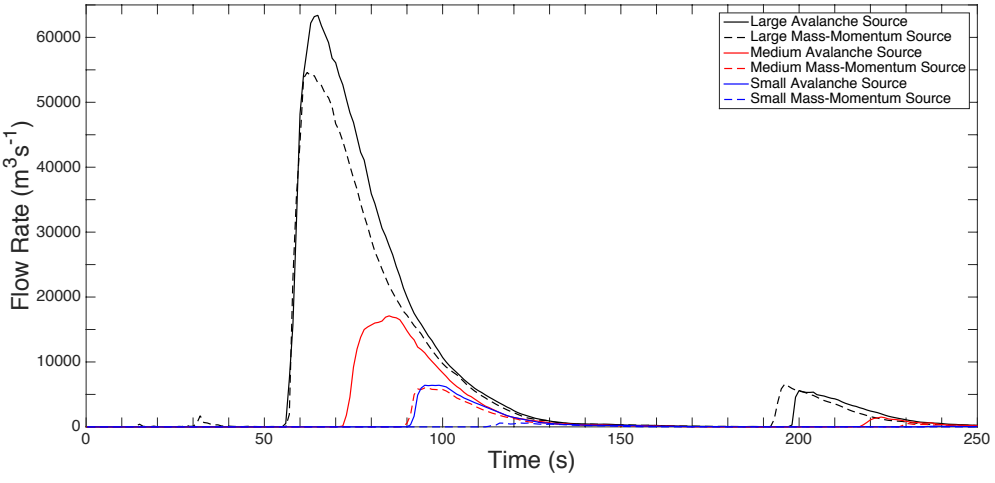

Figure 7. Overtopping wave discharge hydrographs for the three avalanche events and two types of boundary conditions with the lake at the baseline level.

Nat. Hazards Earth Syst. Sci. Discuss., https://doi.org/10.5194/nhess-2017-98
Manuscript under review for journal Nat. Hazards Earth Syst. Sci.
Discussion started: 13 June 2017

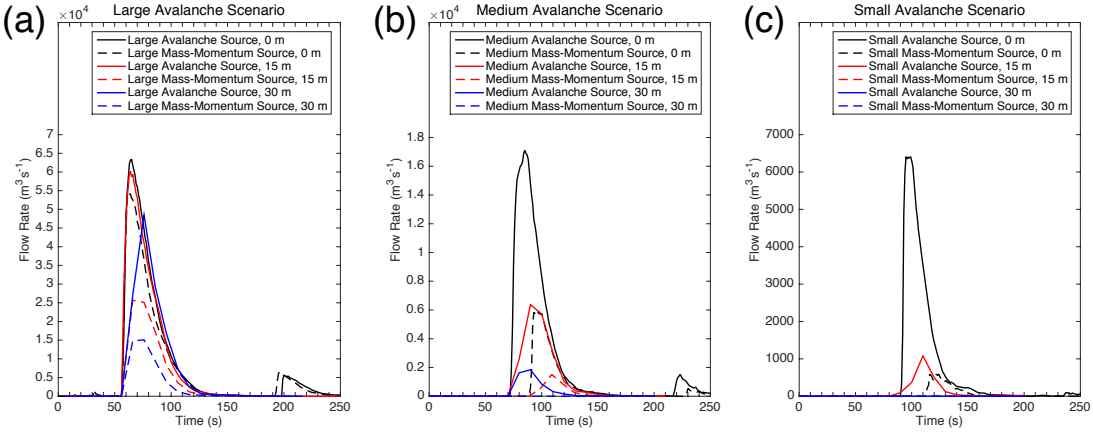

Figure 8. Overtopping hydrographs for lake lowering scenarios for (a) large avalanche scenario, (b) medium avalanche scenario, and (c) small avalanche scenario.